AFRPL TR-86-010

AD:

Interim Report
for the period
20 Sept 1982 to
30 October 1985

Analysis and Measurement of High Frequency Solid Propellant Responses

July 1986

Author:
M. M. Micci

Pennsylvania State University
Department of Aerospace Engineering
233 Hammond Building
University Park, PA 16802

F04611-82-X-0063

Approved for Public Release

prepared for the: **Air Force Rocket Propulsion Laboratory**

Air Force Space Technology Center
Space Division, Air Force Systems Command
Edwards Air Force Base,
California 93523-5000

NOTICE

When U.S. Government drawings, specifications, or other data are used for any purpose other than a definitely related government procurement operation, the government thereby incurs no responsibility nor any obligation whatsoever, and the fact that the government may have formulated, furnished, or in any way supplied the said drawings, specifications, or other data, is not to be regarded by implication or otherwise, or conveying any rights or permission to manufacture, use, or sell any patented invention that may in any way be related thereto.

FOREWORD

This interim report was submitted by the Pennsylvania State University, University Park, Pa, under Contract F04611-82-K-0063 with the Air Force Rocket Propulsion Laboratory (AFRPL). The report includes all work performed from 20 September 1982 to 30 October 1985. Principal Investigator was Michael M. Micci. AFRPL Project Manager was Mr Gary L. Vogt.

This technical report has been reviewed and is approved for publication and distribution in accordance with the distribution statement on the cover and on the DD Form 1473.

GARY L. VOGT
Project Manager

LAWRENCE P. QUINN
Chief, Aerothermochemistry Branch

FOR THE DIRECTOR

ROBERT L. GEISLER
Deputy Chief, Propulsion Analysis Division

SECURITY CLASSIFICATION OF THIS PAGE

REPORT DOCUMENTATION PAGE

AD-A172179

1a. REPORT SECURITY CLASSIFICATION: Unclassified	1b. RESTRICTIVE MARKINGS
2a. SECURITY CLASSIFICATION AUTHORITY	3. DISTRIBUTION/AVAILABILITY OF REPORT: Approved for Public Release; Distribution is Unlimited.
2b. DECLASSIFICATION/DOWNGRADING SCHEDULE	
4. PERFORMING ORGANIZATION REPORT NUMBER(S): None	5. MONITORING ORGANIZATION REPORT NUMBER(S): AFRPL-TR-86-010
6a. NAME OF PERFORMING ORGANIZATION: Michael M. Micci, Dept. of Aerospace Engr. / 6b. OFFICE SYMBOL (If applicable)	7a. NAME OF MONITORING ORGANIZATION: Air Force Rocket Propulsion Laboratory
6c. ADDRESS (City, State and ZIP Code): The Pennsylvania State University, 233 Hammond Building, University Park, PA 16802	7b. ADDRESS (City, State and ZIP Code): AFRPL/DYCR, Edwards AFB, CA 93523
8a. NAME OF FUNDING/SPONSORING ORGANIZATION / 8b. OFFICE SYMBOL (If applicable)	9. PROCUREMENT INSTRUMENT IDENTIFICATION NUMBER: F04611-82-X-0063
8c. ADDRESS (City, State and ZIP Code)	10. SOURCE OF FUNDING NOS.

PROGRAM ELEMENT NO.	PROJECT NO.	TASK NO.	WORK UNIT NO.
62302F	5730	00	BV

11. TITLE (Include Security Classification): ANALYSIS AND MEASUREMENT OF HIGH FREQUENCY SOLID PROPELLANT

12. PERSONAL AUTHOR(S): Micci, Michael Matthew

13a. TYPE OF REPORT	13b. TIME COVERED	14. DATE OF REPORT (Yr., Mo., Day)	15. PAGE COUNT
Interim	FROM 82/9/20 TO 85/10/30	86/7	46

16. SUPPLEMENTARY NOTATION

17. COSATI CODES			18. SUBJECT TERMS (Continue on reverse if necessary and identify by block number)
FIELD	GROUP	SUB. GR.	
21	09	2	Pressure Coupling, Velocity Coupling, Acoustic Admittance, Pressure-Coupled Response, Velocity-Coupled Response, Magnetic Flowmeter.

19. ABSTRACT (Continue on reverse if necessary and identify by block number)

This ~~Interim~~ report describes a ~~research~~ program to study high frequency solid propellant responses. The experimental techniques are based on the application of the magnetic flowmeter. A magnetic flowmeter burner was designed and constructed to evaluate the direct method of pressure-coupled response measurement. Response measurements were obtained for two formulations of AP/HTPB composite propellant at pressure oscillation frequencies from 4000 to 20,000 Hz. The measured data displayed consistent trends in both the real and imaginary parts of the pressure-coupled response function. The unsteady gas phase model of T'ien was ~~utilized~~ used to predict response function trends as a function of frequency. The magnetic flowmeter techniques are currently being applied to the direct measurement of a solid propellant high frequency velocity-coupled response.

20. DISTRIBUTION/AVAILABILITY OF ABSTRACT	21. ABSTRACT SECURITY CLASSIFICATION
UNCLASSIFIED/UNLIMITED ☐ SAME AS RPT. ☒ DTIC USERS ☐	Unclassified

22a. NAME OF RESPONSIBLE INDIVIDUAL	22b. TELEPHONE NUMBER (Include Area Code)	22c. OFFICE SYMBOL
Gary Vogt	805-277-5258	DYCR

DD FORM 1473, 83 APR — EDITION OF 1 JAN 73 IS OBSOLETE.

Unclassified
SECURITY CLASSIFICATION OF THIS PAGE

11. (cont.) RESPONSES (U)

TABLE OF CONTENTS

LIST OF FIGURES

INTRODUCTION

A quantitative knowledge of solid propellant response functions, both pressure-coupled and velocity-coupled, is a critical input parameter for rocket motor stability analyses. There have been several experimental techniques developed to measure propellant pressure-coupled response functions (Refs. 1 & 2). The most widely accepted method for propellant response measurement is the T-burner method. The T-burner has solid propellant placed at the opposing endfaces of a center-vented tube. Pressure oscillations develop between the two propellant surfaces at the fundamental longitudinal frequency of the tube. Pressure-coupled response data is derived by comparing the measured rate of growth and decay of the pressure oscillations. The T-burner is limited to one pressure oscillation frequency for each chamber geometry. A complete investigation over a large range of frequencies requires many different tube lengths. Other methods of measuring the propellant pressure-coupled response incorporate externally driven pressure oscillations in order to examine an entire frequency range with a single burner geometry. One such method utilizes the rotating valve burner. This burner produces pressure oscillations by using a rotating valve to periodically modulate the exit area of the exhaust nozzle. The pressure oscillations within the chamber are a function of the propellant response function and the gas dynamics of the combustion chamber. The magnitude of the pressure oscillations within the combustion chamber is recorded along with the phase angle difference between the pressure and exit area oscillations. The chamber gas dynamics are predicted by an analytical model allowing the solution of the remaining unknown, i.e., the propellant pressure-coupled response.

Another externally driven system employs a traditional acoustic measurement device, the impedance tube. Impedance tube burners use acoustic

drives to generate a standing wave in a combustion tube. The structure of the standing wave is measured by pressure transducers mounted at various points along the length of the impedance tube. The equation that describes the standing wave is derived from the conservation equations applied within the impedance tube and is a function of the propellant admittance. The admittance is deduced by incorporating the pressure measurements into the wave equation.

All of the aforementioned methods result in an indirect measurement of the propellant response function. The pressure-coupled response is derived from a combustion analysis in conjunction with oscillatory pressure measurements. The indirect measurements are only as accurate as the analyses on which they are based. A direct measurement of propellant pressure-coupled response does not require analytical modeling to produce results. One technique utilizing direct measurement is the microwave burner method. This method measures the transient burning rate of solid rocket propellants by reflecting a microwave signal from the burning propellant surface. The oscillatory burning rate can produce the pressure-coupled response when combined with the simultaneous oscillatory pressure measurement. A major drawback to all of the experimental techniques is that they are unable to produce accurate response function measurements at high frequencies (>10 kHz). The problem of high frequency combustion instability has previously been averted by the use of metallic powders which provide excellent high frequency damping. However, in the move toward smokeless propellants, it has become necessary to remove the metal particulates and the problem of propellant response at high frequencies has reappeared.

A magnetic flowmeter is theoretically capable of obtaining a direct measurement of the gas velocity above a burning solid propellant surface with a frequency response greater than 20 kHz. The operation of a magnetic flow

meter is based on the principle first discovered by Faraday in which a conducting gas (or any medium) moving through a magnetic field will generate an electrical potential which is normal to both the magnetic field and the flow velocity. The potential which can be measured as a voltage will be proportional to the magnitude of the flow velocity and to the magnetic field strength. The measurement of the oscillatory gas velocity above a burning solid propellant surface subjected to pressure oscillations constitutes a direct measurement of the propellant pressure-coupled admittance and is the basis of the experimental portion of this program.

The admittance function is defined as the nondimensional ratio of the combustion gas velocity to the oscillatory pressure,

$$A_b = \frac{U_b'/\bar{a}}{P'/\bar{P}} \tag{1}$$

where primes denote fluctuating quantities and superscript bars denote a mean quantity. The oscillatory velocity, U_b', is nondimensionalized by the sonic velocity within the combustion chamber, a. The pressure-coupled response is the nondimensional ratio of the mass flow oscillation to the oscillatory pressure.

$$R_b = \frac{m'/\bar{m}}{P'/\bar{P}} \tag{2}$$

The response and admittance functions are related by the equation,

$$A_b + M_b = \gamma M_b R_b \tag{3}$$

Where M_b is the Mach number of the product gases as they leave the propellant surface and γ is the ratio of specific heats. A magnetic flowmeter is capable

of directly measuring the oscillatory velocity, U_b', which in conjunction with the oscillatory pressure, p', simultaneously measured by a pressure transducer produces the direct measurement of the propellant admittance.

The magnetic flowmeter operates according to Faraday's law which states that an electromotive force, emf, induced in a conductor moving relative to a magnetic field is proportional to the rate at which the magnetic field lines are being passed (Ref. 3). The average emf is defined in equation form as:

$$\text{emf} = -\frac{\Delta\phi}{\Delta t}$$

where $\Delta\phi$ is the change of magnetic flux relative to the moving conductor in a time interval Δt. In the case of a flowmeter, the moving conductor is either a gas or a liquid and the change of magnetic flux is

$$\Delta\phi = BLU\Delta t \tag{5}$$

where B is the magnetic flux density (Telsa), U is the flow velocity (m/s), and L is the distance (m) the emf is being measured across. Therefore, the induced emf expressed in volts becomes

$$V = UBL \tag{6}$$

A calibrating constant is required to account for losses due to nonuniform magnetic fields and other inherent loss mechanisms encountered in the actual application of the magnetic flowmeter.

$$V = \alpha U\beta L \tag{7}$$

The calibration factor, α, is nondimensional and can be determined either theoretically or experimentally. The operating principle of the magnetic flowmeter is presented schematically in Figure 1. Although Equation 7 shows that the potential is independent of flow conductivity, there exist conductivity limits for which the equation holds true. A highly ionized flow could allow magnetohydrodynamic forces to distort the velocity profile. The

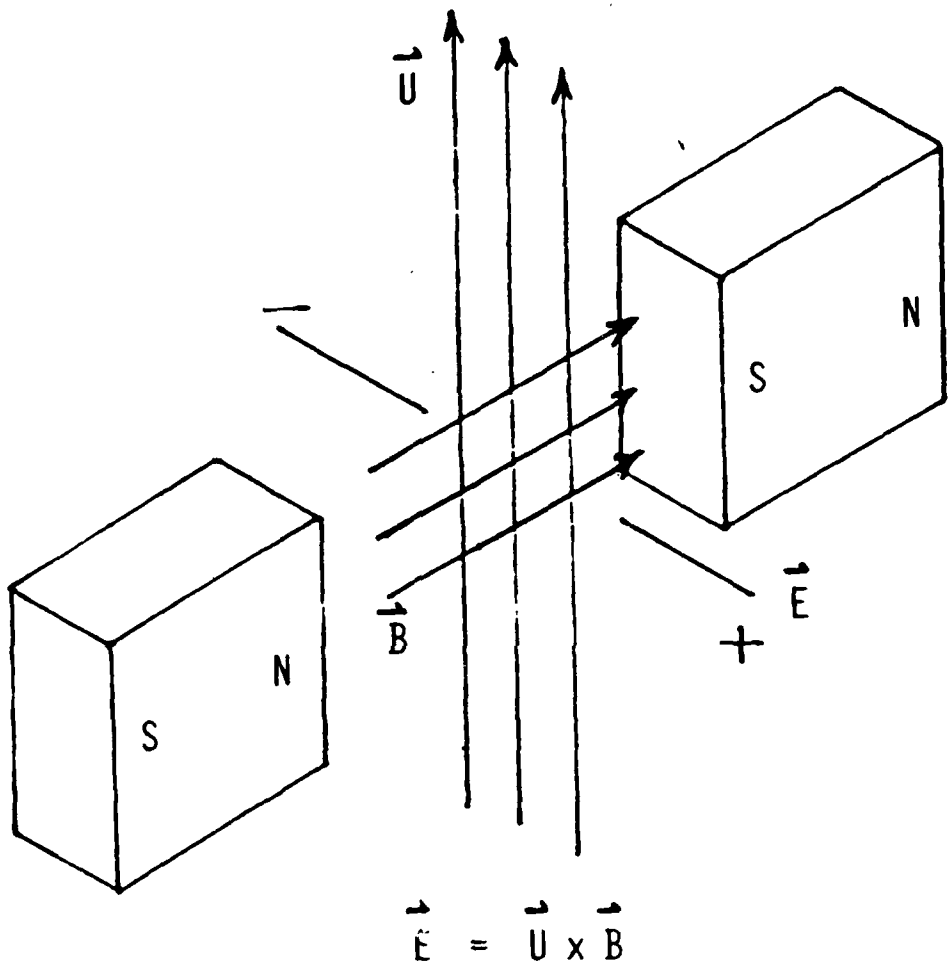

Fig. 1 Principle of operation of a magnetic flowmeter. Induced electric field is proportional to both flow velocity and magnetic field strength.

lower limit for conductivity is approximately 10^{-3} mhos/m, below which the resistance of the conductor becomes as large as the voltage measuring device. Experimental measurements of conductivity in the product gases of solid propellants have been documented for various propellant formulations (Refs. 4 and 5). All of the formulations displayed conductivity levels exceeding the magnetic flowmeter lower limit of 10^{-3} mhos/m.

Both the mean and unsteady interior gas velocities of solid propellant rocket motors were measured by Micci and Caveny (Refs. 6 and 7) using a magnetic flowmeter. The magnetic flowmeter produced well-defined velocity measurements for an AP/HTPB composite propellant in a subscale rocket motor. Longitudinal acoustic waves were generated in the rocket motor by the modulation of the exhaust nozzle area. The oscillatory velocity data permitted the deduction of the propellant pressure-coupled response from a linear analysis of the wave structure. Holme (Ref. 8) investigated the possibility of using magnetic velocimetry for in-flight measurement of rocket exhaust velocity. The magnetic flowmeter technique was tested in this study for several liquid propellant combinations using an alternating magnetic field to eliminate the d.c. effects of chemical polarization.

RESEARCH PROGRAM

PRESSURE COUPLED RESPONSE MEASUREMENTS

The magnetic flowmeter assembly is schematically depicted in Figure 2. This figure presents the major components necessary to measure surface admittances. Pressure oscillations are produced by the pressure modulation system (A) which is located at the converging nozzle orifice. The pressure oscillations and the oscillatory velocity are simultaneously measured as the propellant strand burns by the measurement station shown in the cut-away section (B). The large external magnet (C) provides a large d.c. magnetic field for the velocity measurement obtained by the voltage electrodes at the measurement station. The combustion chamber (D) was designed to consume small amounts of propellant (4.0 cm^3) for each run. The propellant samples were formed into cylindrical strands with a diameter of 1.2 cm and a length of 3.5 cm. The small propellant requirement makes the burner very economical to investigate a wide variety of propellants.

Although commercial magnetic flowmeters use an alternating field in order to separate the flowmeter potential from chemical polarization potentials, a permanent magnet was chosen for the magnetic flowmeter burner. A permanent magnet is well suited for the measurement of an alternating velocity field because any polarization effects (which are low frequency) can be filtered out. The use of a permanent magnet also reduced the complexity of the burner by not requiring additional circuitry to produce a magnetic field. The magnet was an ALNICO 5 permanent magnet which created a magnetic field with a gap density of approximately 2100 gauss. The burner was constructed out of 304 stainless steel which permits the magnetic field to pass through with very little distortion.

The sonic nozzle orifice was modulated by a small toothed gear mounted on

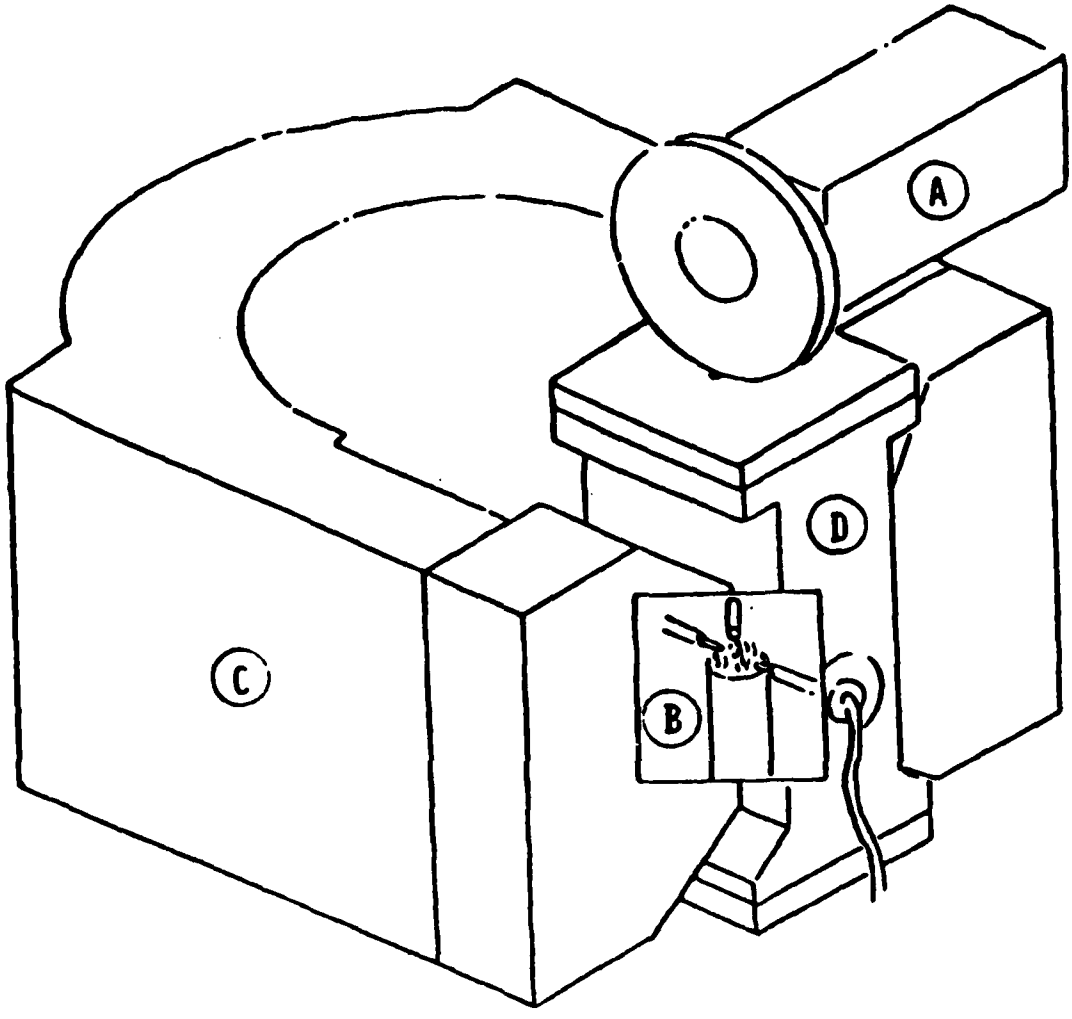

Fig. 2 Isometric view of magnetic flowmeter burner assembly showing propellant burning past pressure and velocity measurement station.

a permanent magnet d.c. motor. The motor speed was controlled by a Variac adjustable autotransformer on an a.c. power line. The a.c. output of the autotransformer was converted to a d.c. voltage for operating the motor. This arrangement permitted steady performance at frequencies ranging from 2000 to 20,000 Hz.

Figure 3 presents a schematic of the data acquisition system utilized for the magnetic flowmeter burner. The oscillatory pressure signal, p', was measured by a PCB model 105A13 pressure transducer with a gain of 100 produced by the PCB model 494A amplifier. A high pass active filter was used to remove all signal noise below 1000 Hz. The signal was then split for recording and used as a reference signal by the vector voltmeter lock-in amplifier. The lock-in amplifier, ITHACO model 393, received the velocity signal directly from the magnetic flowmeter electrodes and isolated the velocity component oscillating at the same frequency as the reference pressure signal. The output of the lock-in amplifier was the magnitude of the velocity oscillation in phase and out of phase with the pressure oscillation. These two measurements generated the real and imaginary parts of the propellant admittance function. The recorded oscillatory pressure was digitized and stored on an IBM PC.

A cold flow simulator was constructed to evaluate the magnetic flowmeter burner design in terms of the magnitude of pressure oscillation and the acoustic characteristics of the combustion chamber. Also, cold flow simulation was necessary to determine any effects the RTV rubber diaphragms had on the transducer frequency response. The simulator duplicated the interior dimensions of the burner with nitrogen gas forced through a porous metal plug to simulate flow from the burning propellant surface at pressure levels up to 14.0 MPa. The same motor and gear pressure modulation system to

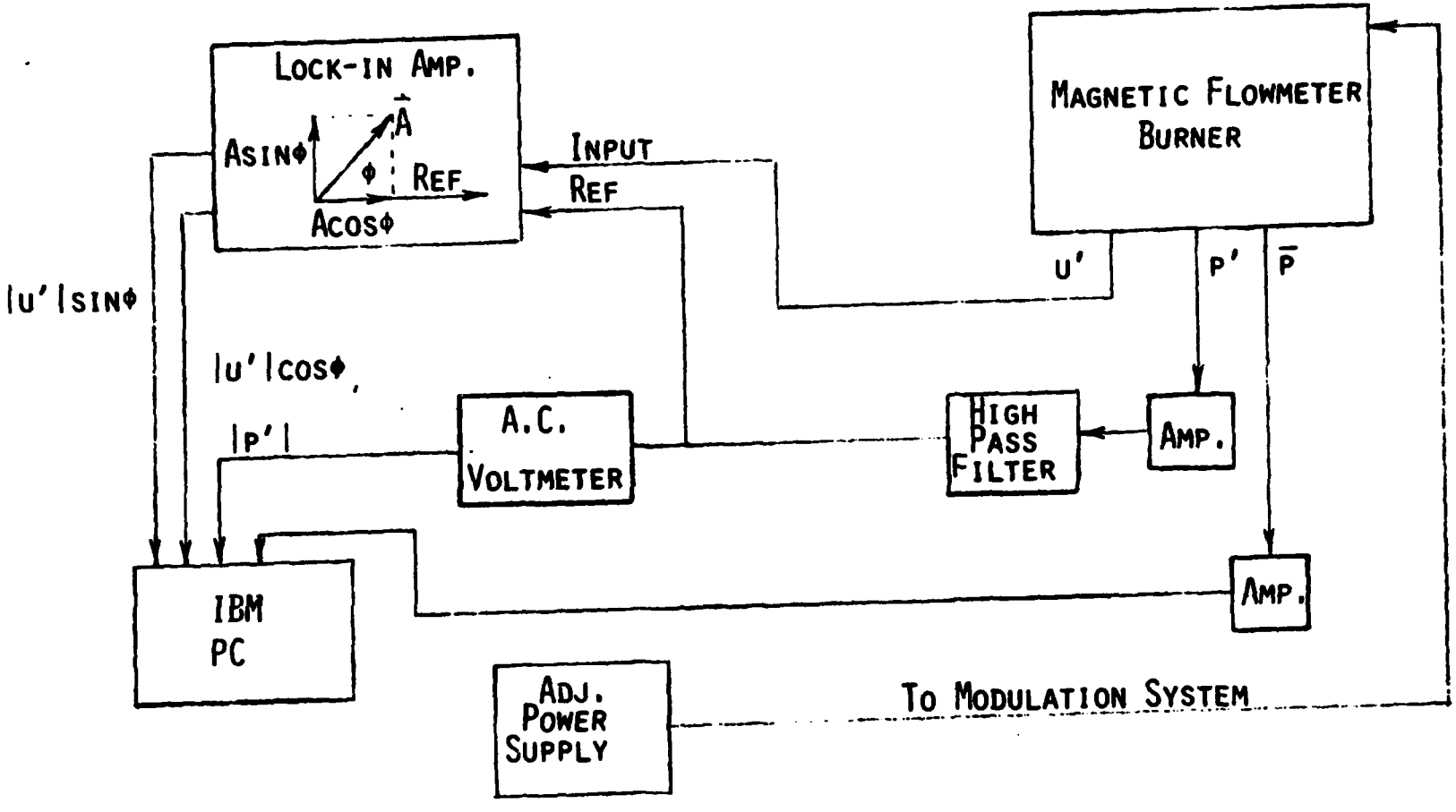

Fig. 3 Data acquisition flowchart.

be used on the burner was applied in the cold flow simulation to determine whether it could produce pressure oscillations of sufficient amplitudes at frequencies up to 20 kHz. The theoretical acoustic characteristics were determined by approximating the chamber as a close ended cylinder.

The performance of the pressure modulation system during cold flow simulation is presented in Figure 4. The pressure oscillation amplitudes produced in the cold flow simulator are plotted as a percentage of mean chamber pressure, $\bar{P}$, at an excitation frequency of 20 kHz. The effectiveness of the exit area modulation declined initially as the mean chamber pressure rose from 1.38 MPa to 6.9 MPa. This behavior is illustrated by the decline in the oscillatory to mean pressure ratio in Figure 4. The pressure ratio remained essentially constant from 6.9 MPa to 13.8 Mpa at a value of approximately 0.7%. The amplitude of pressure oscillation was dependent on the mean chamber pressure and the gap between the nozzle exit plane and the teeth of the rotating gear. The optimum gap distance was found to be approximately 3.0 millimeters. A slight increase in this distance resulted in a large reduction in the oscillation amplitude.

The cold flow simulator was also used to test the effectiveness of RTV rubber diaphragms of different thicknesses. These diaphragms were necessary to protect the pressure transducer during the combustion of the propellant. The results of these tests are plotted in Figure 5. The diaphragm thicknesses were 1.5 mm and 3.0 mm and they were compared to an unprotected transducer over a frequency range of 4,000 Hz to 20,000 Hz. The mean chamber pressure was held constant at 3.4 MPa. The diaphragms caused an amplitude loss which was dependent on the excitation frequency, but the phase angle between the protected and the unprotected transducers remained zero. Identical results were obtained for the two thicknesses at every frequency. Based on these

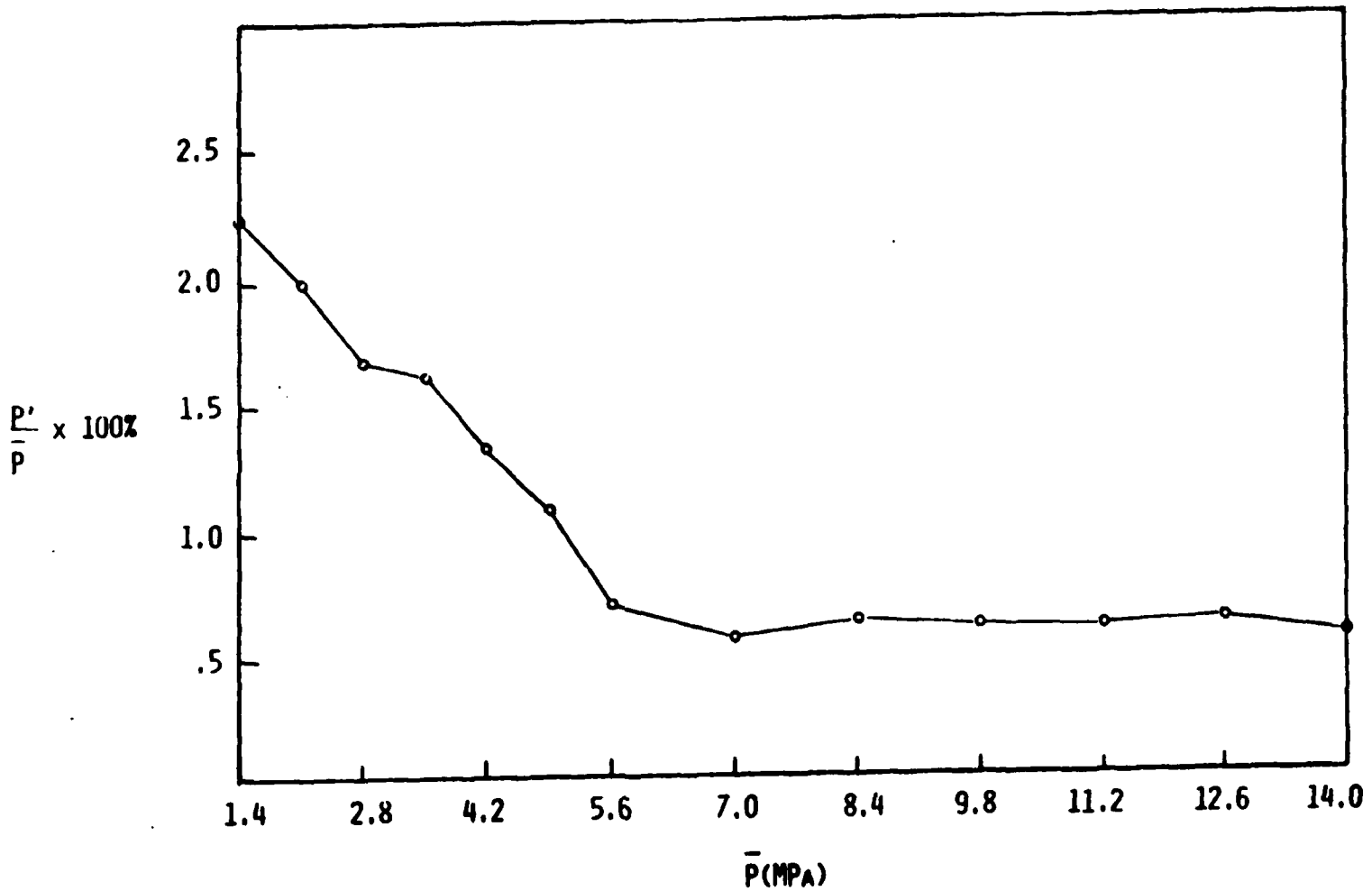

Fig. 4 Pressure oscillation amplitude versus mean chamber pressure at an excitation frequency of 20 kHz.

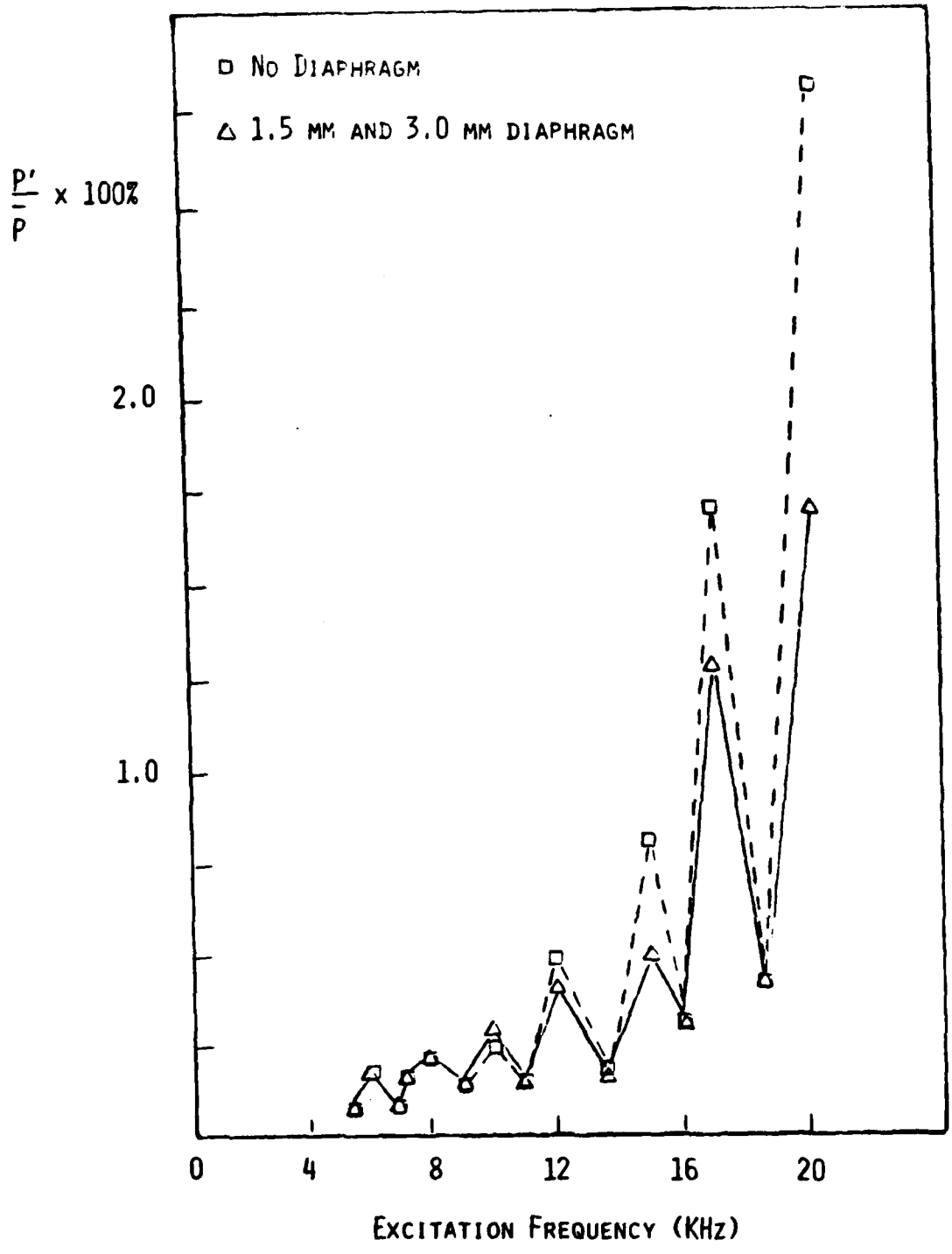

Fig. 5 Pressure oscillation amplitude versus excitation frequency for two diaphragm thicknesses at a mean chamber pressure of 3.4 MPa.

experimental results and design factors, the smaller diaphragm thickness was selected for use in the magnetic flowmeter burner. Figure 5 also displays the cold flow resonant modes. The observed amplitude peaks at frequencies less than 16,000 Hz correspond to the predicted harmonic resonant frequencies for longitudinal mode oscillation. The first observed amplitude peak occurred near the second harmonic frequency for longitudinal mode oscillations with additional peaks occurring near each consecutive resonant frequency up to the sixth longitudinal harmonic of 15,720 Hz. Tangential mode oscillation occurred at frequencies above 16000 Hz creating resonant modes which were combinations of tangential and longitudinal oscillations. These combination modes were observed at two predicted resonant frequencies of 17,098 Hz and 19,885 Hz.

The validity of the response function measurements relies on the accurate calibration of the magnetic flowmeter for both velocity signal amplitude and phase. The amplitude calibration consisted of determining the calibration constant, α, in Equation 4. This was achieved by a device designed to simulate the velocity measurement in the magnetic flowmeter burner. The conducting gas flow in the burner was replaced by a solid copper rod with a diameter of 6.0 mm. The conductivity independence of the magnetic flowmeter equation permitted this replacement as long as the gas flow conductivity was above the limit of 10^{-3} mhos/m. An electromagnetic shaker oscillated the copper rod in the magnetic field produced by the ALNICO 5 permanent magnet. Two graphite brushes picked up the potential across the rod induced by the conductor moving through the magnetic field. The amplitude of the a.c. potential was measured by the lock-in amplifier which used a reference signal provided by the shaker power supply. The velocity of the rod was derived by integrating the acceleration measurement of a PCB model 305A05 accelerometer

mounted on the top of the copper rod. The calibration data was recorded as flowmeter voltage versus oscillatory velocity of the calibration device. This data was very consistent over a wide range of velocity amplitudes. The ratio between velocity and voltage was inserted into Equation 4 along with the measured magnetic field strength, B, and the electrode separation, L, yielding a calibration constant of 2.1.

The velocity phase calibration was required to correct the phase shift induced by the inherent capacitance of the measuring circuit combined with the high gas resistance. The capacitance induces an appreciable phase shift in the velocity signal if the resistance of the combustion gas products is large. To quantatively determine the phase shift that occurred in the course of the experiments, the combustion gas resistance had to be measured. Direct measurement of the gas resistance using an ohmmeter created polarization of the electrodes, therefore, an indirect method was employed to determine the gas resistance. In this method the resistance was experimentally determined by measuring the phase shift induced on an oscillatory signal passed through the combustion gas products. The advantages of this arrangement are that it utilized the same equipment configuration as the magnetic flowmeter burner and did not require the replacement or alteration of the existing combustion chamber. Excellent run to run agreement was achieved for the gas resistance measurements obtained at several frequencies of oscillation, with the mean value of gas resistance being 40,000 ohms. The value for the gas resistance produced a maximum phase shift in the velocity measurement of 35.6 degrees at a measurement frequency of 20,000 Hz.

All propellant tested was of 80% AP and 20% HTPB composition. The first response function data was obtained for a 20 μm unimodel AP particle size at a modulation frequency of 8000 Hz. Figures 6a and 6b plot the real and

imaginary parts respectively of the pressure-coupled response for this propellant formulation. The data is plotted as a function of distance above the burning propellant surface. The maximum distance plotted, 1.6 mm, corresponds to the diameter of the velocity measurement electrode. Mean pressures for the tests ranged from 4.5 to 8 MPa and are listed for each test on Figures 6 through 11. At the pressures shown in Figures 6a and 6b, the propellant burn rate was 0.58 cm/s. The real part of the response in Figure 6a displays excellent reproducibility. The sampling rate was increased to obtain better spatial resolution for testing of a 200 μm AP particle size propellant. Figures 7a and 7b show the real and imaginary parts respectively of the pressure-coupled response at a modulation frequency of 4000 Hz. The value for the real part remains fairly constant while the imaginary part displays a change in value through the flame zone. Figures 8a and 8b show the real and imaginary parts at a modulation frequency of 8000 Hz. For these tests the sampling rate was increased to its then maximum obtainable value of 250 Hz. At this frequency, the real part of the response increases with distance above the propellant surface while the imaginary part remains constant at a slight negative value. At the chamber pressures shown in Figures 7 and 8 the 200 μm AP propellant burn rate was approximately 0.7 cm/s.

Additional pressure-coupled measurements were made by two undergraduate students for their senior thesis project. Measurements were made at modulation frequencies of 12, 16, and 20 kHz for the 200 μm unimodal AP propellant. Difficulties were encountered obtaining a sufficiently high signal-to-noise ratio and the data exhibited greater scatter than at the lower modulation frequencies. Figures 9a and 9b plot the real and imaginary parts respectively of the pressure-coupled response at a modulation frequency of 12,000 Hz. The data for the two runs at this frequency show agreement for the

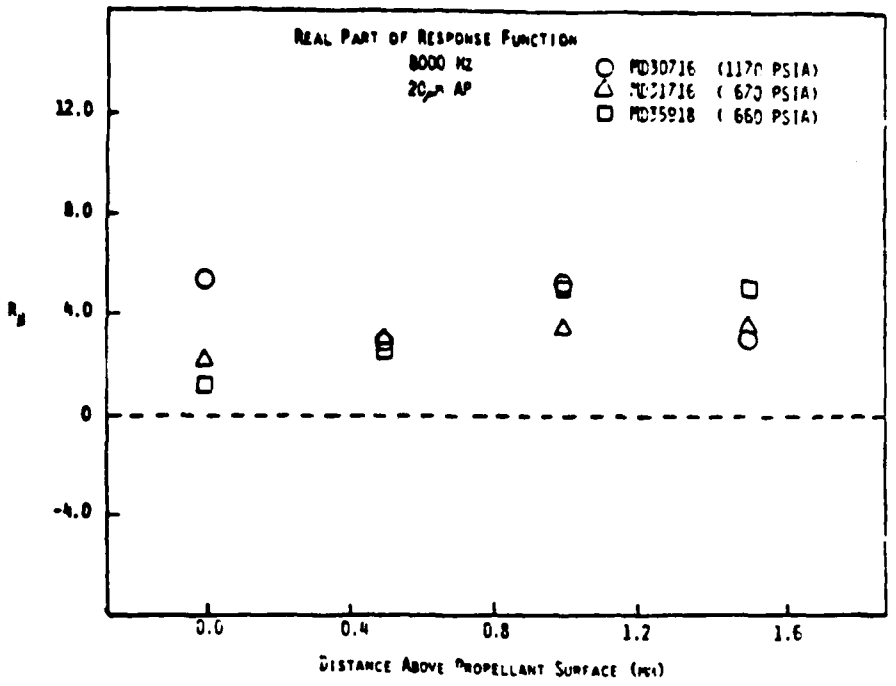

Fig. 6a Real part of pressure-coupled response as a function of distance above propellant surface for 20 μm AP propellant tested at 8000 Hz.

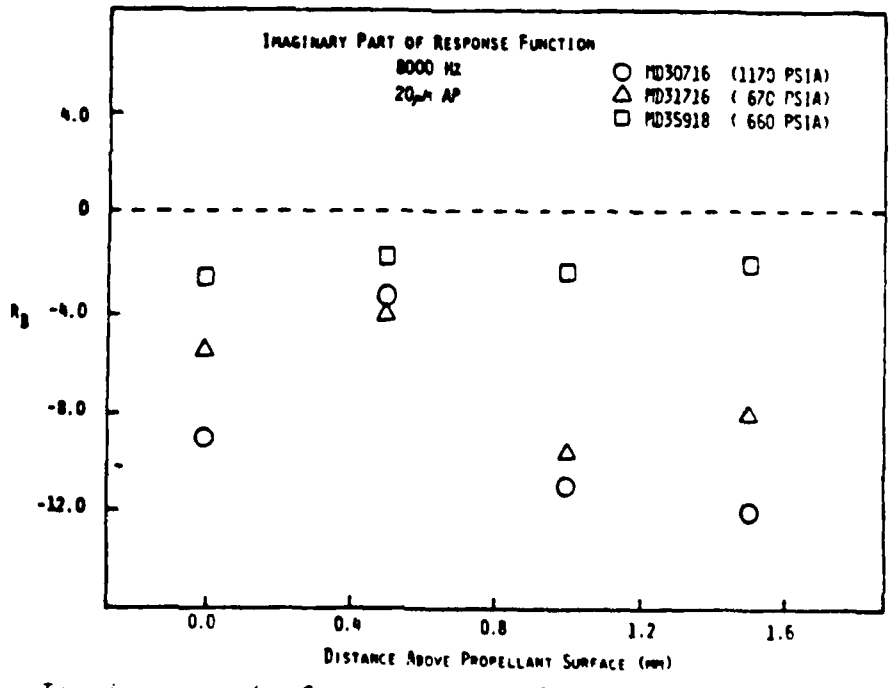

Fig. 6b Imaginary part of pressure-coupled response as a function of distance above propellant surface for 20 μm AP propellant tested at 8000 Hz.

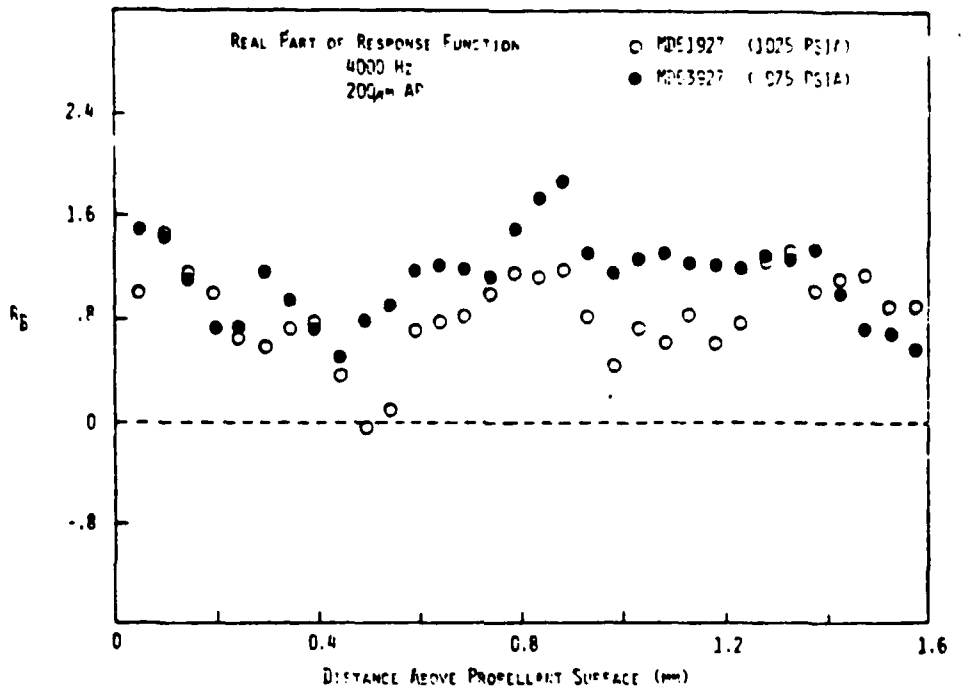

Fig. 7a Real part of pressure-coupled response as a function of distance above propellant surface for 200 μm AP propellant tested at 4000 Hz.

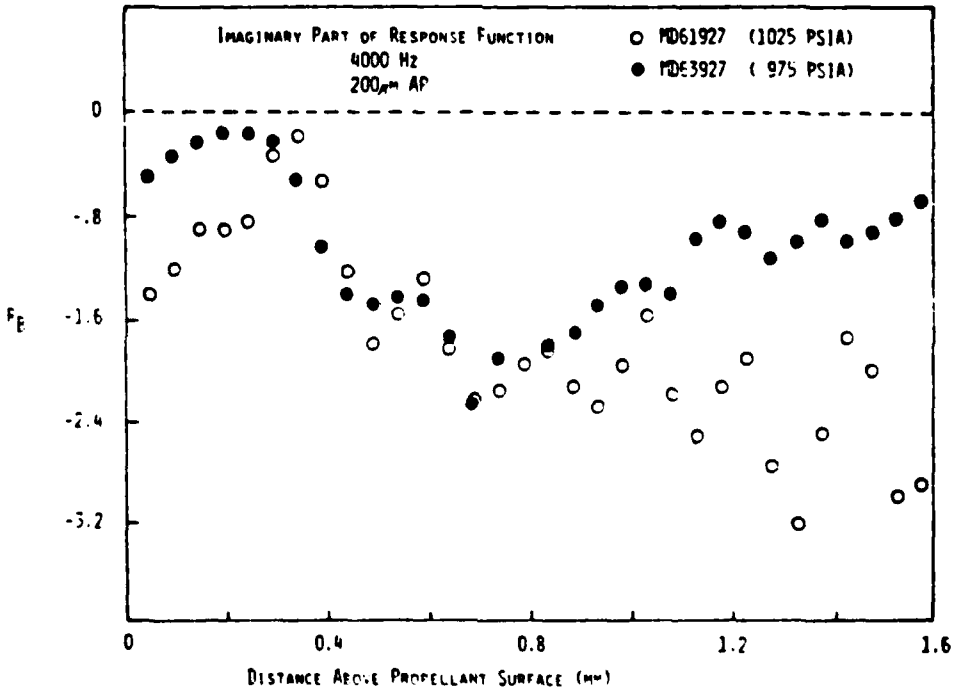

Fig. 7b Imaginary part of pressure-coupled response as a function of distance above propellant surface for 200 μm AP propellant tested at 4000 Hz.

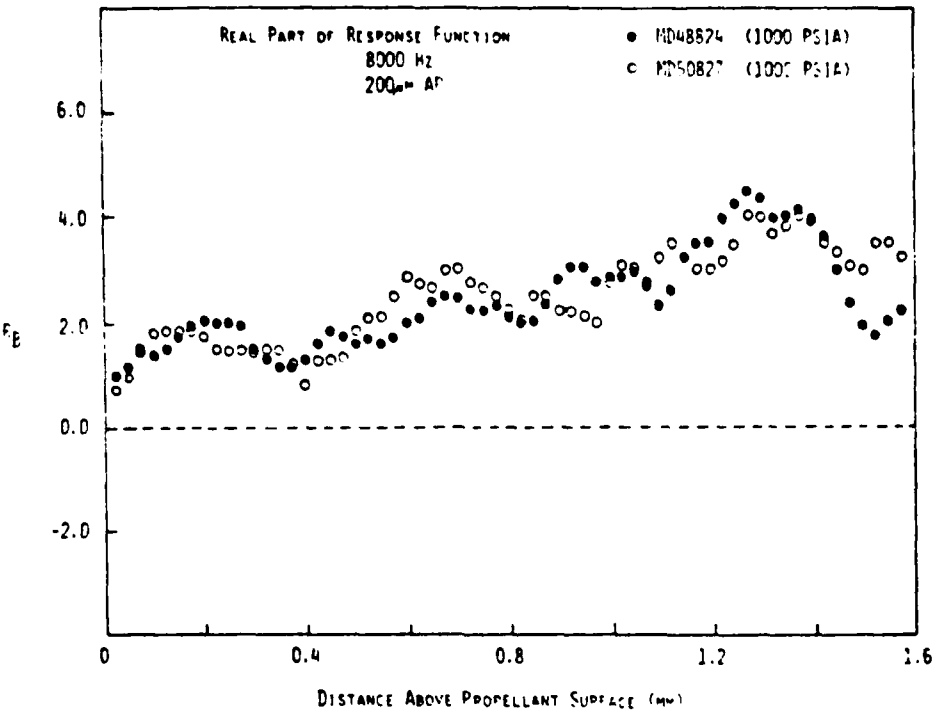

Fig. 8a Real part of pressure-coupled response as a function of distance above propellant surface for 200 μm AP propellant tested at 8000 Hz.

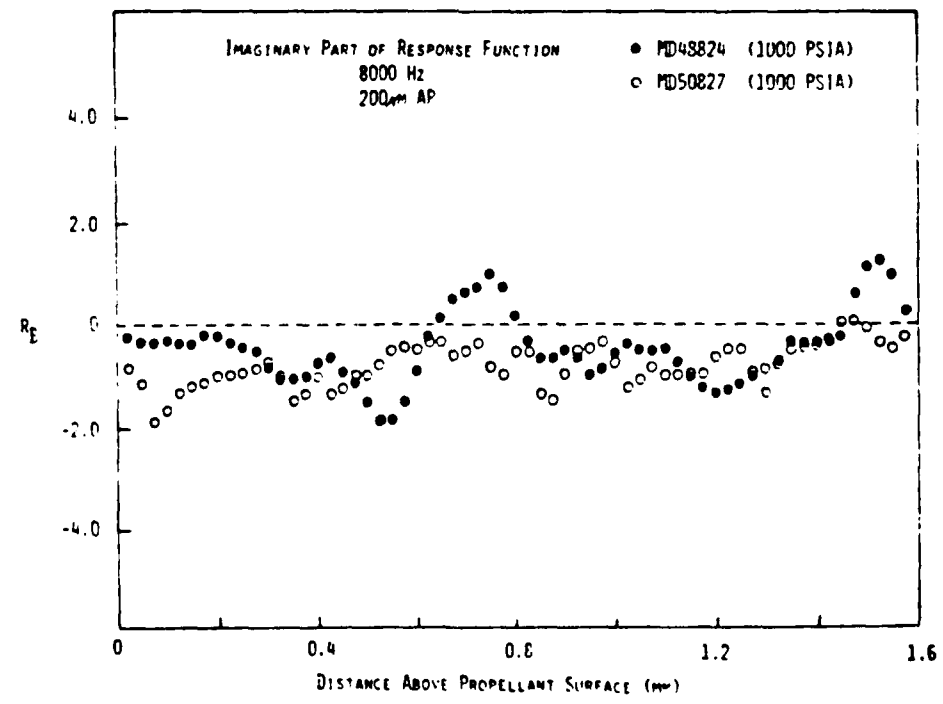

Fig. 8b Imaginary part of pressure-coupled response as a function of distance above propellant surface for 200 μm AP propellant tested at 8000 Hz.

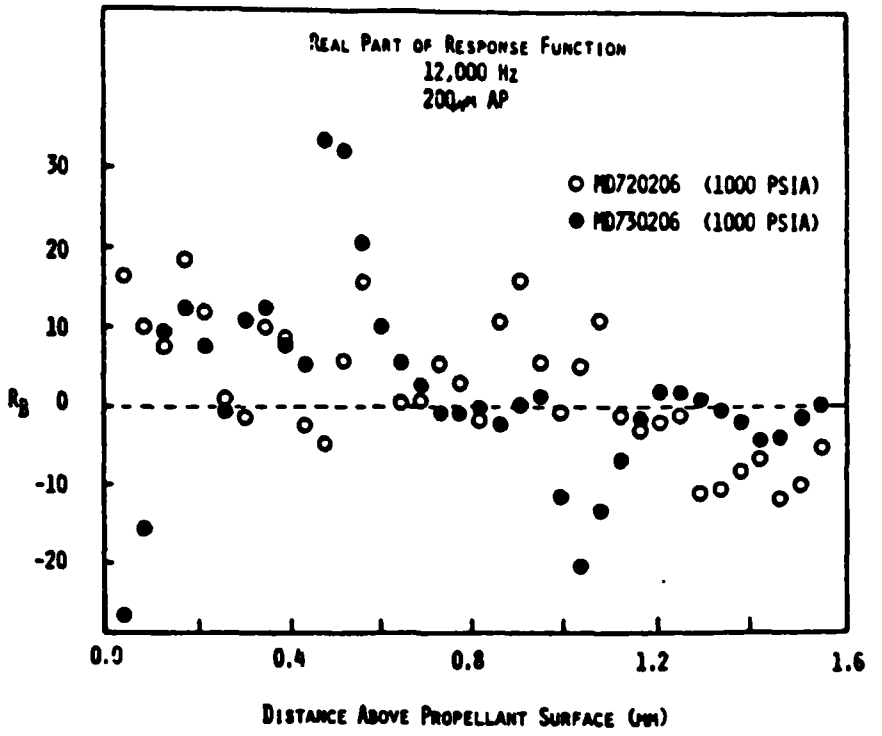

Fig. 9a Real part of pressure-coupled response as a function of distance above propellant surface for 200 μm AP propellant tested at 12,000 Hz.

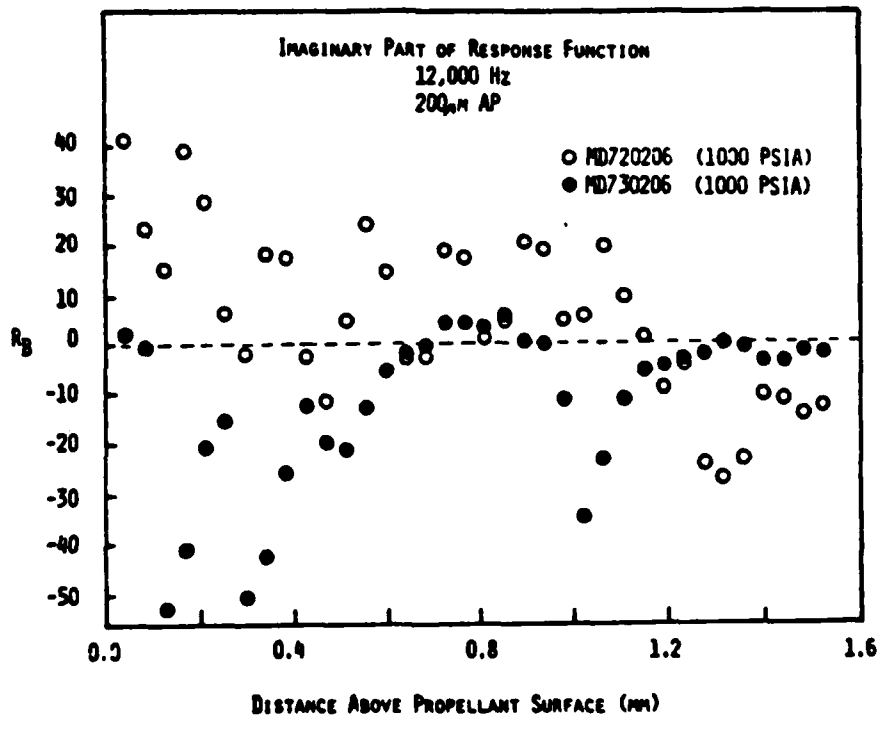

Fig. 9b Imaginary part of pressure-coupled response as a function of distance above propellant surface for 200 μm AP propellant tested at 12,000 Hz.

real part, however, agreement cannot be claimed for the imaginary part. Figures 10a and 10b show the real and imaginary parts respectively of the pressure-coupled response at a modulation frequency of 16,000 Hz. Agreement between the two runs made at this frequency was not obtained for either the real or imaginary parts. Figure 11 plots both the real and imaginary parts of the pressure-coupled response for the one run made at a modulation frequency of 20,000 Hz. Depletion of the supply of 200 μm unimodal AP propellant prevented additional testing at these high frequencies. At the chamber pressures shown in Figures 9 through 11, the propellant burn rate was approximately 0.7 cm/s.

PRESSURE-COUPLED RESPONSE ANALYSIS

The effort to obtain an analytical model for predicting the high frequency solid propellant response functions follows the method used by Tien (Ref. 9). This method numerically integrates a fifth order system of ordinary differential equations. The flame is assumed to be one-dimensional, premixed, laminar, and a one-step forward chemical reaction is taking place. The specific heats, molecular weights, and coefficient of heat conduction are taken to be constant, and the Lewis number is equal to unity. The governing equations for the reacting flow above the solid propellant surface are continuity, energy, and specie conservation given by

$$\frac{\partial \rho}{\partial t} + \frac{\partial \rho u}{\partial x} = 0 \tag{8}$$

$$\rho \frac{\partial T}{\partial t} + \rho u \frac{\partial T}{\partial x} - \frac{\partial^2 T}{\partial x^2} - \frac{\gamma - 1}{\gamma} \frac{\partial p}{\partial t} = wq \tag{9}$$

$$\rho \frac{\partial Y_i}{\partial t} + \rho u \frac{\partial Y_j}{\partial x} - \frac{\partial^2 Y_i}{\partial x} = \nu_j w$$

$$i = f,o,p \tag{10}$$

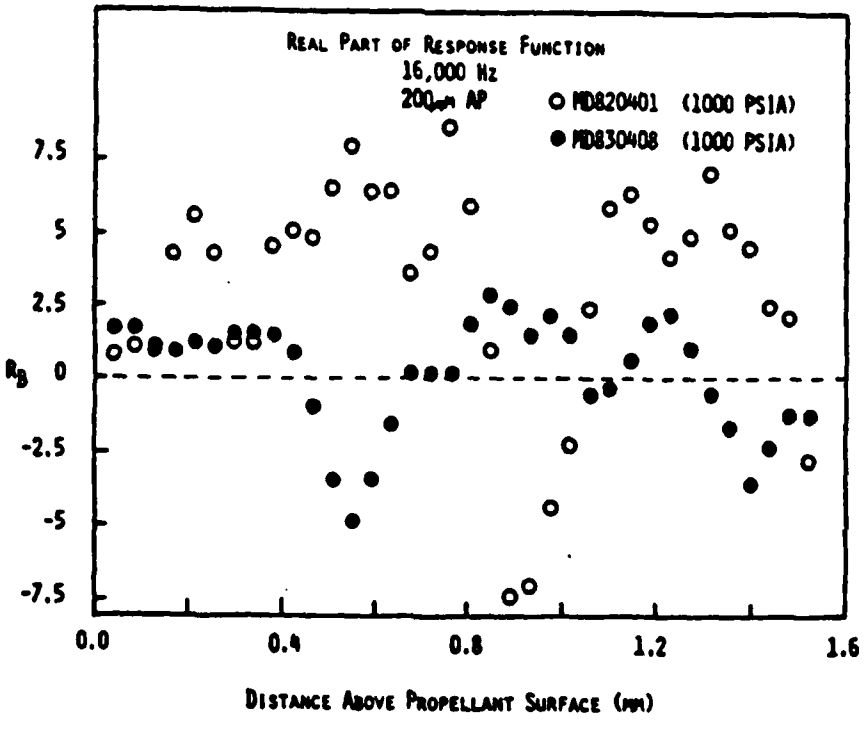

Fig. 10a Real part of pressure-coupled response as a function of distance above propellant surface for 200 μm AP propellant tested at 16,000 Hz.

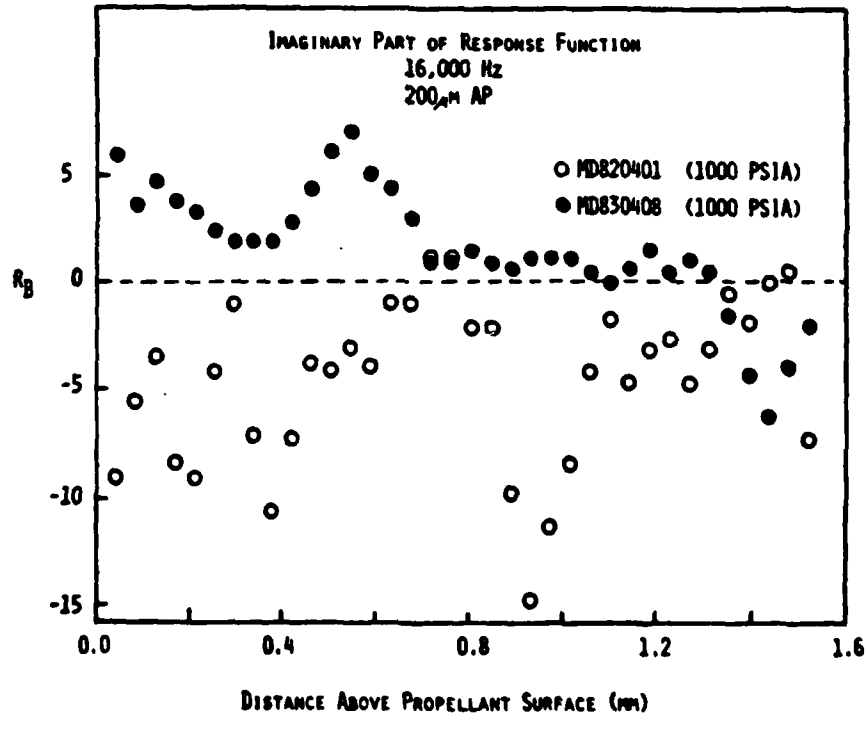

Fig. 10b Imaginary part of pressure-coupled response as a function of distance above propellant surface for 200 μm AP propellant tested at 16,000 Hz.

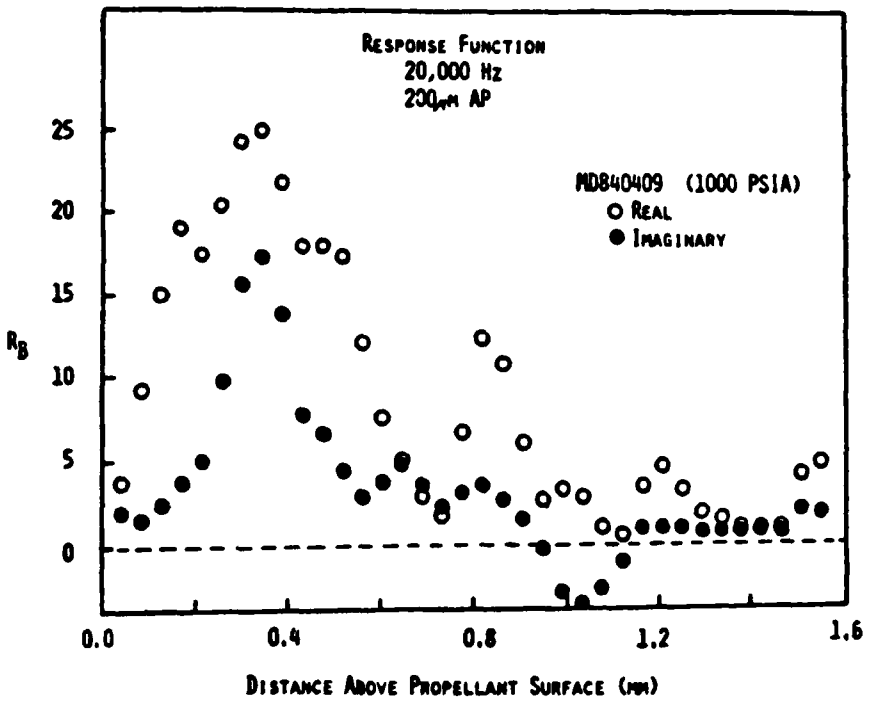

Fig. 11 Real and imaginary parts of pressure-coupled response as a function of distance above propellant surface for 200 μm AP propellant tested at 20,000 Hz.

where w is the reaction rate, q is the heat of reaction, ν_j is a function of the reaction stoichrometric coefficients and the molecular weight of the species, and Y is the mass fraction. A perturbation analysis was utilized with a small amplitude sinusoidal time oscillation assumed for the variable and with both mean and perturbation quantities being functions of height above the burning propellant surface. Since the pressure wave length is always much larger than the flame thickness, the pressure was assumed to be a function of time only and a momentum equation is not required. Tien's model is the only one to assume an unsteady gas phase reaction in addition to the unsteady heat transfer to the burning solid propellant. The boundary condition equations resulted from solving the energy equation in the solid phase and by assuming an isentropic flow very far from the flame.

A fourth order Runge-Kutta method was utilized to integrate from the outer flame edge, $x = \infty$, to the propellant surface, $x = 0$. The integration was carried out in this direction to allow a linear conversion method to be used to calculate the boundary values. The linear conversion method separated the solution into homogeneous solutions and a particular solution (Ref. 10). Each of the homogeneous solutions was expressed in terms of the $x = \infty$ boundary value. The dependent variable for each homogeneous solution was given an initial boundary value of unity and a value of zero for the particular solution. The system of equations was then integrated for each set of boundary values. The resulting solutions were summed and placed in the boundary equations to determine the correct boundary values of $x = \infty$.

Figure 12 plots the mean temperature and reaction rate as a function of distance above the burning propellant surface which is at location $x = 0$. These curves were obtained by integrating the mean energy equation and are required as input for the integration of the perturbation equations. The

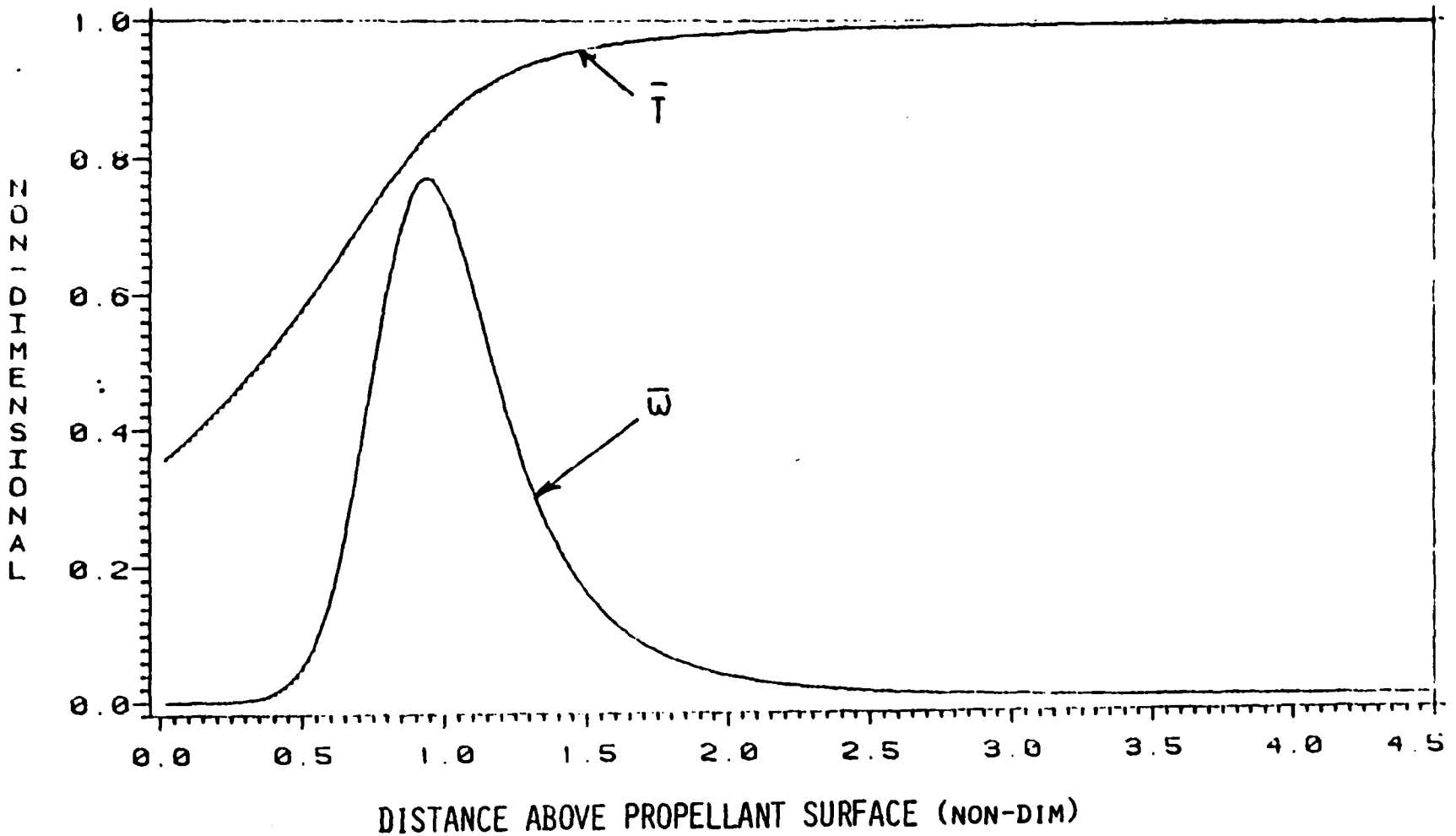

Fig. 12 Steady-state distributions of temperature, $\bar{T}$ and reaction rate, $\bar{\omega}$, across the flame.

results given by the unsteady gas phase model of T'ien were then compared with the pressure-coupled admittances measured for the 200 μm unimodel AP composite propellant at 4000 and 8000 Hz. The model was utilized to calculate the oscillating velocity component, u', versus height above the burning propellant surface through the flame zone for comparison with experimentally measured values. The two key parameters which were varied are the nondimensionalized frequency, ω, and the ratio of gas residence time to the solid residence time, Σ. Figure 13 shows a representative result for ω=2 and Σ=0.0122. It can be seen that the model predicts a real component of the fluctuating velocity that levels out at a constant value with increasing distance from the propellant surface while the imaginary component steadily becomes more negative with increasing distance. This compares with the experimental data shown in Figure 7. Σ and ω were then varied to determine if the T'ien model could reproduce the functional dependence of the admittance on the frequency of the pressure oscillations. Figure 14 shows the real part of the admittance for two frequencies a factor of two apart. It can be seen that for the Σ of 0.0244 the higher frequency produces a higher real part of the admittance. This was also observed experimentally as can be seen by comparing Figures 7 and 8. However, the model still predicted an imaginary part with a constant negative slope unlike the measured value for the imaginary part shown in Figure 8 at a frequency of 8000 Hz. It is felt at this time that the T'ien model is too simplistic in the chemical reaction kinetics to accurately model all the observed behavior of the solid propellant admittance.

VELOCITY-COUPLED RESPONSE MEASUREMENTS

A burner to measure solid propellant velocity-coupled responses was designed based on the knowledge gained from operation of the pressure-coupled

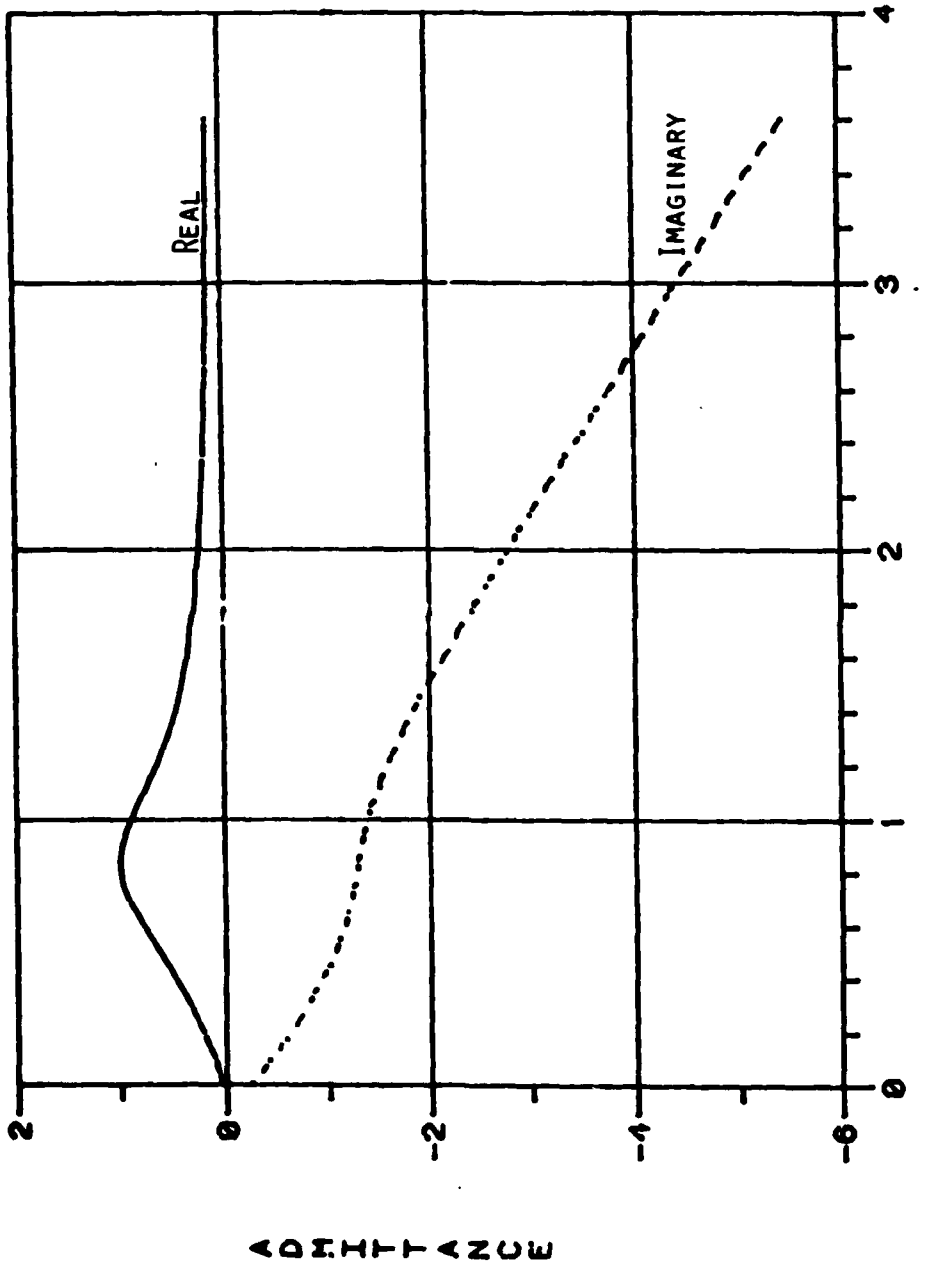

Fig. 13 Real and imaginary parts of the admittance as a function of nondimensional distance above the burning propellant surface ($\Sigma = 0.012$, $\omega = 2$).

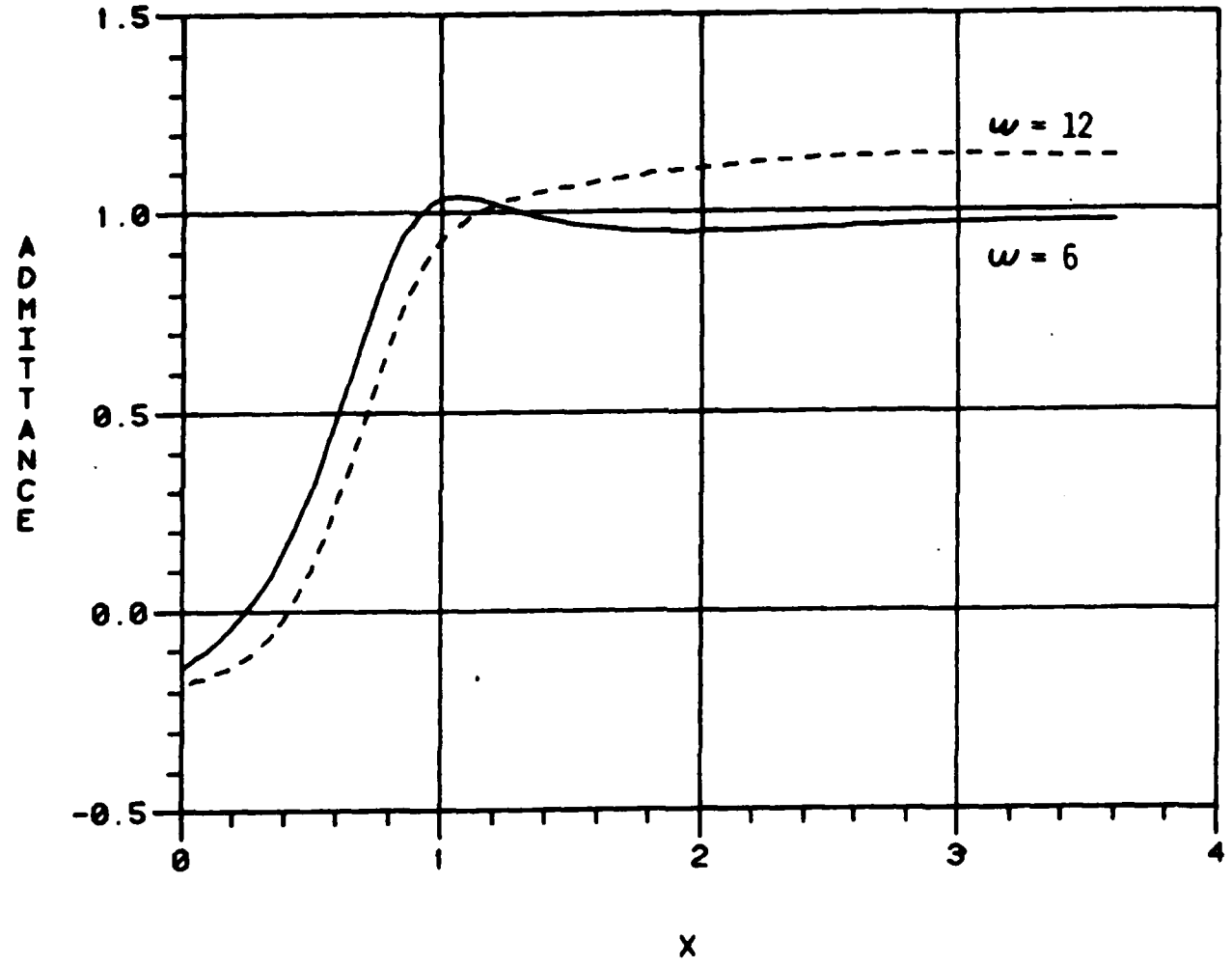

Fig. 14 Real part of the admittance as a function of nondimensional distance above the burning surface for two values of the frequency, ω.

burner. Here the velocity-coupled response is defined to be the response of the propellant burning rate to an oscillatory cross-flow velocity adjacent to the propellant surface. Figure 15 shows the propellant geometry and the orientation of the electrodes and magnetic field to permit the simultaneous measurement of the cross-flow oscillating velocity, V', and the oscillatory velocity of the gas leaving the propellant surface, U_b'. It is a 2-D slab motor with two pairs of velocity measuring electrodes embedded in two facing propellant slabs. Three of the electrodes penetrate one propellant slab with the fourth electrode in the opposing slab. One pair of electrodes will measure the cross-flow velocity above the propellant surface (V') and the other pair will measure the velocity of the hot combustion gasses leaving the propellant surface (U_b'). Correlating the two measurements will give the velocity-coupled response. Figure 16 shows the velocity-coupled magnetic flowmeter burner. A is the burner assembly, B is the permanent magnet, C is a cutaway view of the propellant slabs and velocity electrodes and D is the rotating toothed gear used to modulate the burner orifice and generate a standing wave in the combustion chamber. The velocity measurement station is located at the midpoint of the chamber where a velocity antinode and a pressure node would be situated for a standing wave at or near the chamber fundamental longitudinal frequency. This was done in order to maximize the oscillatory cross-flow velocity to obtain a high signal-to-noise ratio and to minimize pressure oscillations which would generate a pressure-coupled response. The electrodes are rigidly mounted and the height of the measurement station above the burning propellant surface increases as the propellant regresses, ranging during a burn from 0 to 9 mm at burnout. Figure 17 is a detailed drawing of the velocity-coupled magnetic flowmeter burner showing the locations of the mean chamber pressure transducer, the electric

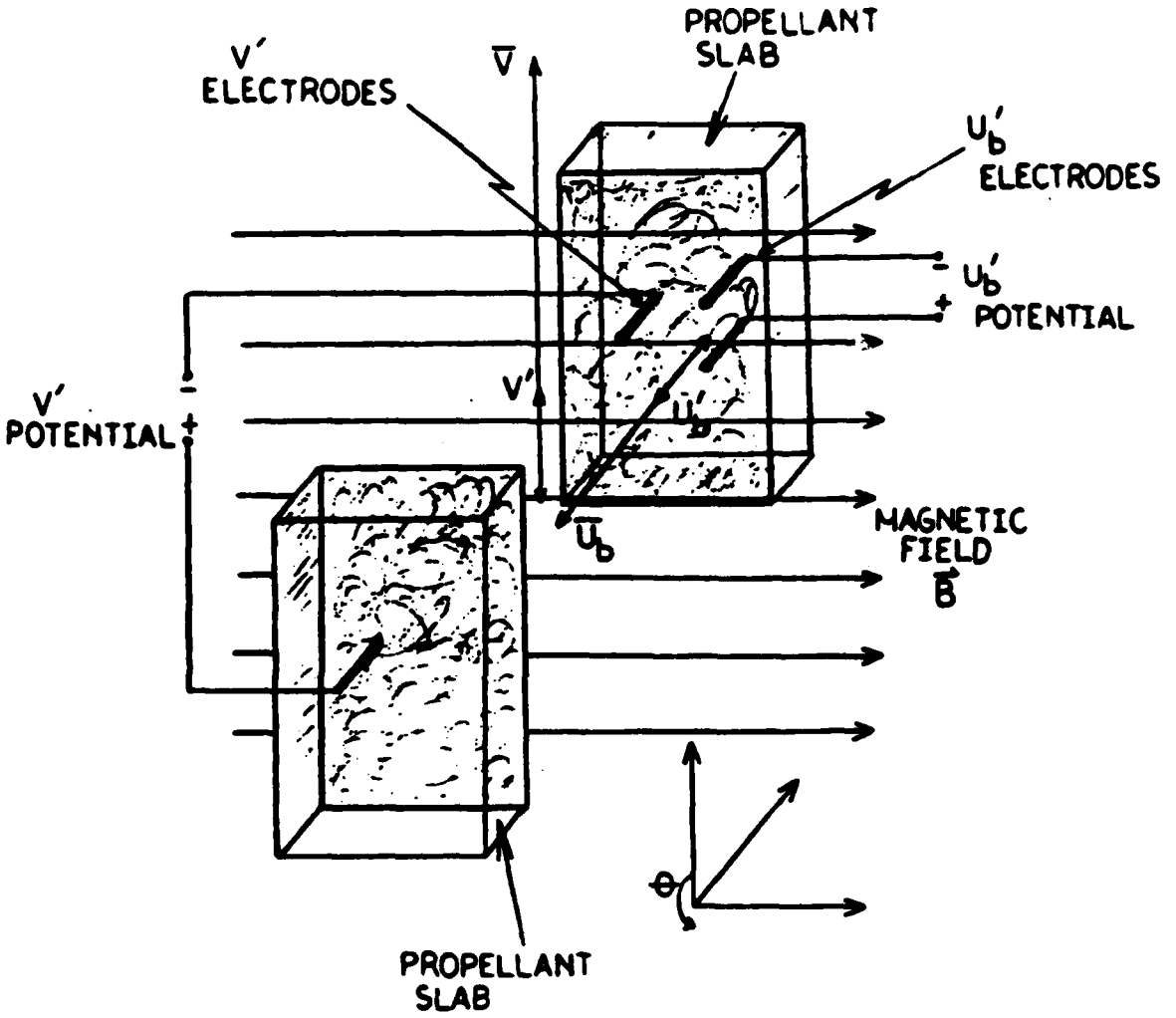

Fig. 15 Slab propellant geometry and orientation of electrodes and magnetic field for the simultaneous measurement of the oscillatory cross-flow velocity, V′ and the oscillatory velocity of the gas leaving the propellant surface, U_b'.

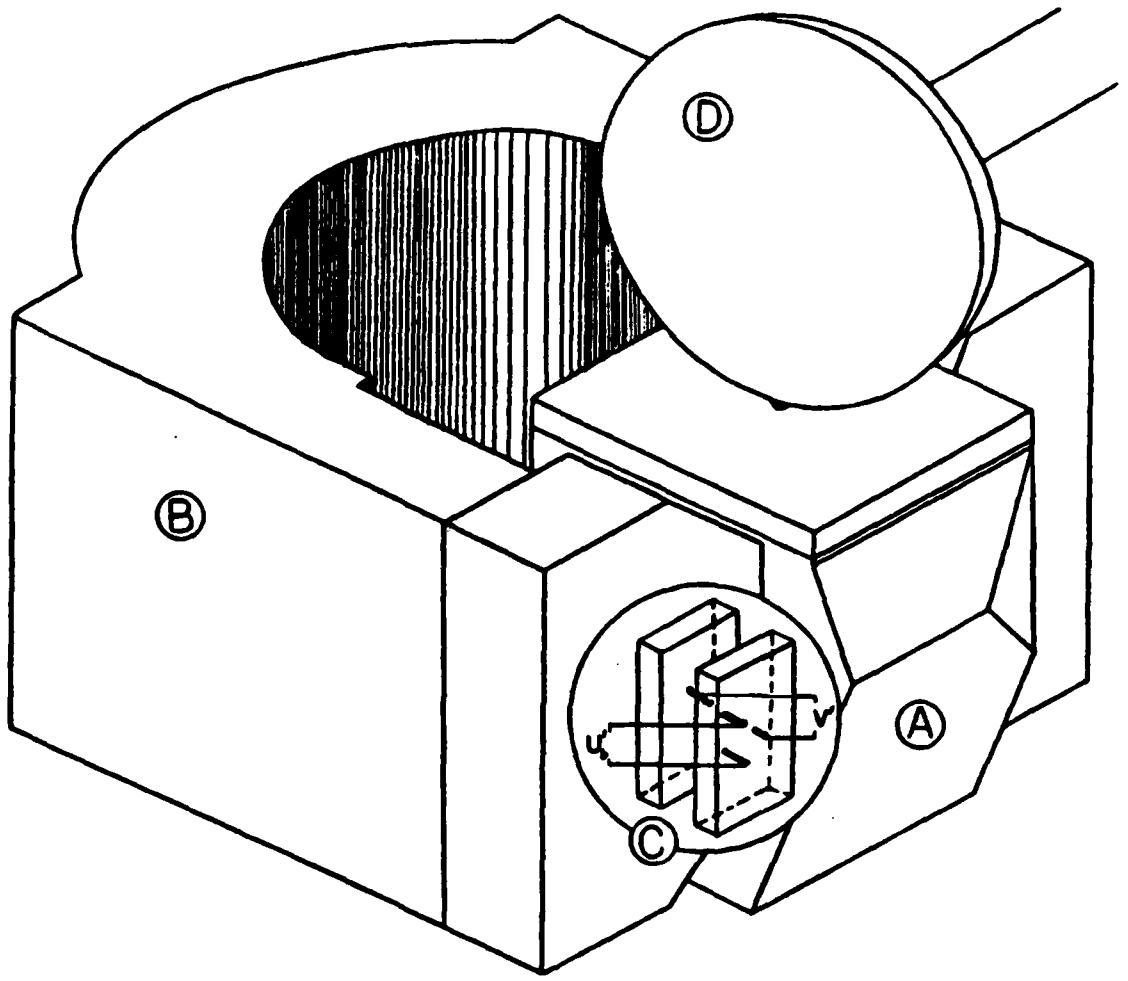

Fig. 16 Velocity-coupled magnetic flowmeter burner used to make simultaneous measurement of oscillatory cross-flow velocity, V', and oscillatory velocity of gas normal to propellant surface, U_b'. Components: A-burner assembly, B-permanent magnet, C-cutaway view of propellant slabs and velocity electrodes, D-rotating toothed gear.

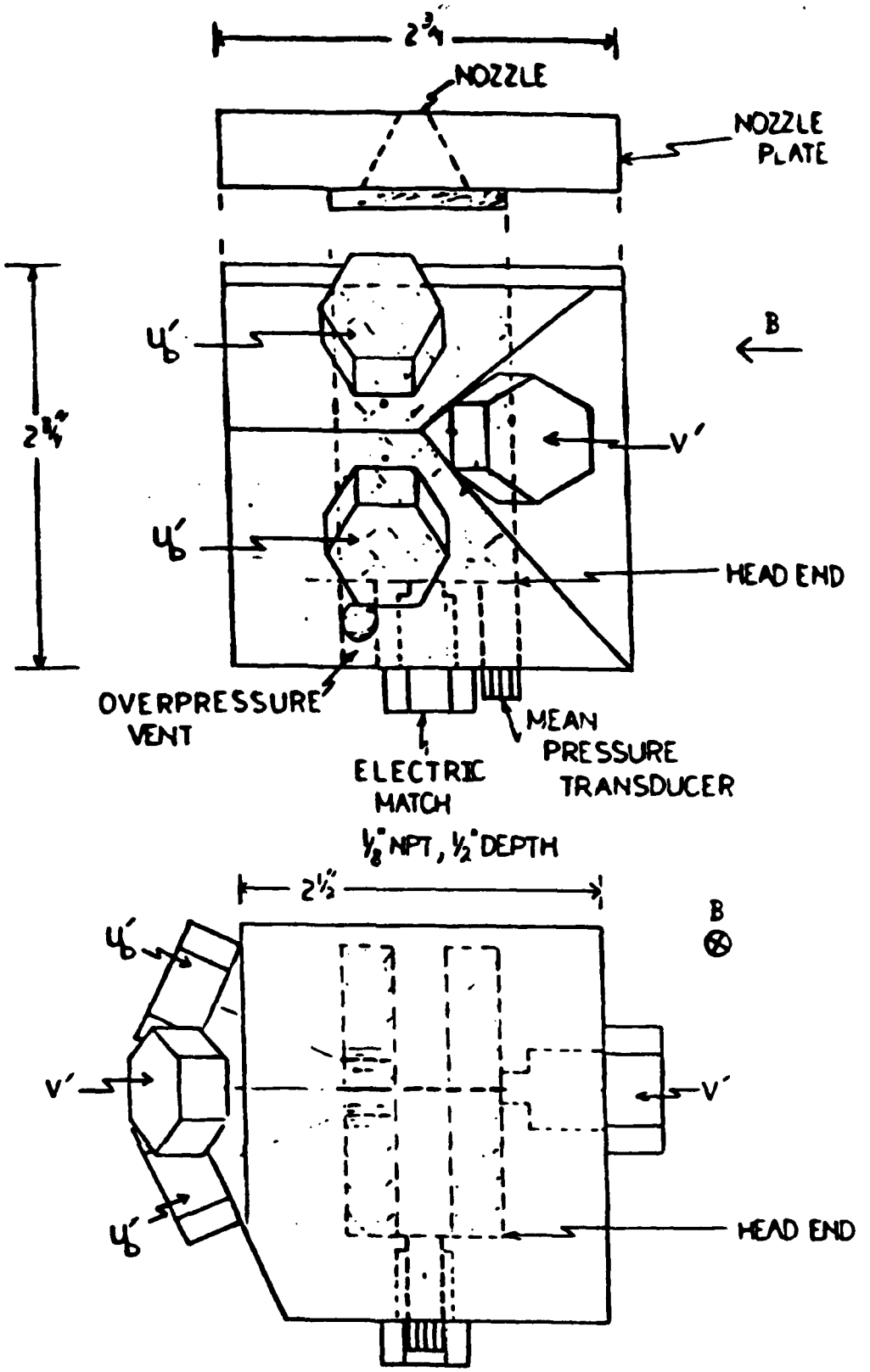

Fig. 17 Velocity-Coupled Magnetic Flowmeter Burner.

match used for ignition and the overpressurization vent at the head end of the chamber and the sonic nozzle at the opposite end. Velocity-coupled response data is currently being obtained with this device.

CONCLUSIONS AND RECOMMENDATIONS

There are two major shortcomings for the methods presently used to measure solid propellant pressure-coupled response functions. They are unable to produce reliable results at high frequencies (> 10 kHz) and the majority of the methods rely on an indirect means of response function measurement. One of the objectives of this study was to develop an apparatus that utilizes a magnetic flowmeter to obtain direct measurements of the pressure-coupled response functions for solid propellants. The device was required to perform these measurements over a frequency range up to 20,000 Hz while consuming small amount of propellant. A burner apparatus was designed and constructed to meet these specifications. A magnetic flowmeter was incorporated in the apparatus in order to measure the velocity fluctuations of the combustion gas products occurring during unsteady combustion of solid propellant samples. This velocity measurement was the essential feature of the magnetic flowmeter burner because it permits the pressure-coupled response function to be obtained directly from the experimental data.

The magnetic flowmeter burner provided pressure-coupled response measurements for two formulations of AP/HTPB composite propellant at selected frequencies. The AP particle size differed between the two formulations, 20 μm AP and 200 μm AP. The magnetic flowmeter provided oscillatory velocity measurements as the electrodes were exposed to the combustion gas products. Mean and oscillatory pressure measurements were recorded simultaneously with the oscillatory velocity measurements. These measurements produced the surface admittance function for the burning propellant samples. A simple relationship produced the pressure-coupled response function from the admittance function. Repeatable behavior was noted in the real and imaginary parts of the pressure-coupled response for the 20 μm AP and 200 μm AP

propellant samples.

The validity of the response function measurements relies on the accurate calibration of the magnetic flowmeter. The magnitude of the oscillatory velocity signal was readily calibrated by the data generated by the velocity calibration device. This data was consistent over a wide range of velocity amplitudes. The velocity phase shift correction was found to be dependent on the combustion gas resistance. The resistance was experimentally determined by measuring the phase shift induced on an oscillatory signal passed through the combustion gas products. The advantages of this arrangement are that it utilizes the same equipment configuration as the magnetic flowmeter burner and did not require the replacement or alteration of the existing combustion chamber. Excellent run to run agreement was achieved for the gas resistance measurements obtained at several frequencies of oscillation.

The magnetic flowmeter burner satisfied the objective of this experimental study by producing direct pressure-coupled response function measurements. The burner proved capable of measuring pressure-coupled response at frequencies beyond the limits imposed on other methods. The small amount of propellant consumed by the magnetic flowmeter burner for each run makes the technique very economical for extensive testing of various solid propellants. Some difficulty was experienced with obtaining the measurement of the oscillatory velocity at a frequency other than the resonant frequency. This problem did not seriously hamper the effectiveness of the magnetic flowmeter burner and can most likely be remedied by minor design modifications.

The external method of inducing pressure oscillations within the combustion chamber of the burner produced smaller than expected amplitudes and the oscillatory pressure signal was subjected to d.c. shifts due to

temperature effects and partial exhaust nozzle blockage. A high pass filter and an 100 gain amplifier was incorporated into the circuit to condition the oscillatory pressure signal. The improved pressure signal was inadequate for the lock-in reference signal. The small pressure oscillations resulted in velocity measurements with a low signal-to-noise ratio. Measurements at an excitation frequency of 8000 Hz were of sufficient amplitude to be readily distinguished from background noise. This was due to the excitation frequency being near the first longitudinal resonant frequency of the combustion chamber. Cold flow simulation has shown that the oscillation amplitude is much larger at the chamber resonant frequencies. However, the velocity signal was of the same order of magnitude as the noise at frequencies other than resonant frequencies. The velocity signal was harder to discern for the burner tests at other frequencies. The test had to be repeated several times to verify the data. A method to increase the velocity signal or reduce the amount of background noise is needed before effective measurements can be taken at other frequencies.

Magnetic flowmeter burner effectiveness can be improved by modifying the chamber design to allow a larger diameter propellant strand. Additional propellant consumption would be offset by the benefits. A larger exit nozzle orifice size would accomodate the larger diameter propellant strands tested over the same range of mean chamber pressures. Nozzle blockages by combustion residue will decrease and mass flow through the nozzle will increase. The greater mass flow permits higher amplitude pressure oscillations generated by the pressure modulation system. In addition to an improved reference signal for the lock-in amplifier, the larger oscillations within the combustion chamber will increase the velocity measurements by the magnetic flowmeter.

Another benefit of the larger diameter propellant strands involves the

effect of the velocity electrodes embedded in the strands. The propellant burning surface deforms around the electrodes as they are exposed by the receding propellant. The calibration of the flowmeter velocity measurements assumes an uniform flow vector from a planer burning surface. This assumption is rendered invalid if large deformities alter the average propellant surface level. The effect of the deformities caused by the electrodes would be less significant on a larger burning surface area.

The unsteady gas phase analysis of T'ien has been used to successfully predict the trends of the pressure-coupled response as a function of frequency. The model numerically integrates the governing equations, continuity, energy and specie conservation, to predict the mean and oscillating components of the flow variables: velocity, temperature, and specie mass fractions. Numerical results and experimentally measured pressure-coupled response values are compared. However a more accurate combustion process model is necessary to quantitatively predict the propellant high frequency pressure-coupled response.

Techniques validated in the pressure-coupled magnetic flowmeter burner were applied to design and construct a high frequency velocity-coupled magnetic flowmeter burner. Two pairs of velocity electrodes simultaneously measure oscillatory cross-flow velocity and oscillatory gas flow velocity normal to the propellant surface. The geometry utilized was a two-dimensional slab motor. The sonic nozzle is modulated to generate a fundamental mode standing wave in the chamber with the measurements station located at the velocity antinode. Experimental data is currently being taken to determine the ability of the magnetic flowmeter technique to measure a velocity-coupled response.

REFERENCES

1. Brown, R. S., Click, F. E. C., and Zinn, B. T., "Experimental Methods for Combustion Admittance Measurements," Progress in Astronautics and Aeronautics: Experimental Diagnostics in Combustion of Solids, Vol. 63, AIAA, New York, N.Y., 1978, pp. 191-220.

2. Levine, J. N., and Andrepont, W. C., "Measurement Methods of Transient Combustion Response Characteristics of Solid Propellant - An Assessment," AIAA Paper 79-1209, June 1979.

3. Semat, H., Fundamentals of Physics, 4th ed., Holt, Rinehart and Winston, Inc., New York, N.Y., 1966.

4. Capener, E. L., Chown, J. B., Dickinson, L. A., and Nanevicy, J. E., "Studies on Ionization Phenomena Associated with Solid-Propellant Rockets," AIAA Journal, Vol. 4, No. 8, August 1966, pp. 1349-1354.

5. Bestgen, R. F., A Study of the Effects of Electrical Fields on Solid Propellant Burning Rates, AFRPL-TR-71-87, Air Force Rocket Propulsion Laboratory, Edwards AFB, CA, July 1971.

6. Micci, M. M., and Caveny, L. H., "MHD Measurement of Acoustic Velocities in Rocket Motor Chambers," AIAA Journal, Vol. 20, No. 4, April 1982, pp. 516-521.

7. Micci, M. M., "Solid Propellant Response Functions Deduced by Means of Forced Longitudinal Waves in Rocket Motors," Ph.D. Thesis, Dept. of Mechanical and Aerospace Engineering, Princeton University, 1981.

8. Holme, J. C., Investigation of an Electromagnetic Technique for the Independent Measurement of Chemical Rocket Exhaust and Vector, AFRPL-TR-65-98, Astrosystems International, Inc., Fairfield, NJ, June 1965.

9. Tien, J. S., "Oscillator Burning of Solid Propellants Including Gas Phase Time Lag," Combustion Science and Technology, Vol. 5, 1972, pp. 47-54.

10. Na, T. Y., Computational Methods in Engineering Boundary Value Problems, Academic Press, New York, N.Y., 1979.